ELSEVIER

Contents lists available at ScienceDirect

## Chemical Engineering Journal

journal homepage: www.elsevier.com/locate/cej





# Molecular insights of condensate trapping mechanism in shale oil reservoirs and its implications on lean gas enhanced oil recovery

Shihao Wang <sup>a,\*</sup>, Hongwei Zhang <sup>b</sup>, Bikai Jin <sup>a</sup>, Rui Qiao <sup>b</sup>, Xian-Huan Wen <sup>a</sup>

- <sup>a</sup> Chevron Technical Center, Chevron, 1400 Louisiana Street, Houston, TX 77002, USA
- <sup>b</sup> Department of Mechanical Engineering, Virginia Tech, Blacksburg, VA 24061, USA

#### ARTICLE INFO

Keywords: Capillary trapping Adsorption Enhanced oil recovery Shale oil Molecular simulation Gas injection

#### ABSTRACT

The heterogeneous pore structure and the confinement effect of the narrow pore space lead to the differential release/retention phenomenon of hydrocarbons in unconventional reservoirs. So far, the mechanism of this phenomenon, in particular the dynamic process, requires further investigation since it affects the design of gas-based enhanced oil recovery (EOR) operations. In this work, we aim to numerically study the capillary condensate trapping mechanism that causes the differential release phenomenon by conducting molecular dynamics (MD) simulations.

In our work, a two-bath MD model is set up, in which two baths are used to mimic the bulk pores and a nanochannel connecting the two baths is used to model the pore throat. Methane (C1) and decane (C10) molecules are used to represent the light and heavy component of the in-situ oil. The MD results show that at the early stage of the primary depletion, the light components release faster than the heavier components, leading to increasing gas oil ratio (GOR) above the system's bubble point. As depletion continues, heavier hydrocarbons accumulate in the nano-channel due to the confinement effect, while light hydrocarbons tend to remain in the dead-end pores. During the gas EOR process, the injected gas 'dissolves' the liquid in the nano-channel and thus enhances the recovery of the 'trapped' hydrocarbons.

This work systematically investigates the impact of pore throat on the differential release and trapping effect. We demonstrate that a significant amount of light hydrocarbons may be 'trapped' during the primary depletion of unconventional reservoirs, due to the capillary condensate trapping effect. The trapped hydrocarbons can be partly recovered through gas injection. Our study has implications for practical EOR operations.

#### 1. Introduction

Unconventional shale reservoirs are rich resources of hydrocarbons. In general, shale rocks contain organic matters and inorganic matters. The organic matters, also known as 'kerogen', are believed to be the birthplace of hydrocarbons. The permeability of shale reservoirs is significantly lower than that of the conventional reservoirs [1]. Due to the low permeability, the production rate of shale reservoirs declines rapidly during the primary depletion stage. It has been reported in the literature [2,3] that the recovery efficiency of unconventional reservoirs could be below 5 %, resulting in huge amount of hydrocarbons trapped in the reservoirs. Therefore, it is of critical importance for the petroleum community to understand the trapping mechanism as well as to enhance the production of shale reservoirs. The diameter of a fraction of pores in the shale rocks is in the nano-meter level, causing the transport of

hydrocarbon molecules within them to be impacted by the nano-confinement. The transport dynamics is further complicated by the selective adsorption [4] and retention effect [5] for different hydrocarbon components. In our previous works, we have investigated the transport dynamics of gas phase mixtures [6] and liquid phase mixtures [7] in the shale and tight reservoirs, respectively. In [8], the mechanism of carbon dioxide enhanced recovery of shale gas reservoirs is studied at the molecular level and it was found that carbon dioxide particularly enhances the recovery of heavier components in a hydrocarbon mixture. In [9], the flow behavior of hydrocarbon mixtures through a single kerogen slit was studied using MD simulation, and it was found that asphaltene molecules demonstrates strong adsorption capability in the nano channel, causing the flow/velocity distribution to be inhomogeneous. In Zheng et al. [10], the primary depletion and gas huff-n-puff of (light) hydrocarbon mixtures in organic and inorganic slits were studied

E-mail address: shihao.wang@chevron.com (S. Wang).

<sup>\*</sup> Corresponding author.

numerically. They further confirmed the differential release effect of hydrocarbons with different weights and found that the wall materials significantly affect the transport behavior. Zhao et al. [11] used molecular simulations to study the behavior of water displacing an oil-filled pore throat, and compared it with the traditional Young-Laplace equation. Luo et al. [12] developed a pore-size-dependent equation of state and used it to study the lean gas injection in shale gas-condensate reservoirs. They found that due to the selectively release of lighter hydrocarbons from the nano pores, heavier components with reduced critical points tend to accumulate in the nano pores. Although significant progress has been made, the transport behavior of hydrocarbon mixtures through a pore throat is still not well understood. Particularly, the compositional effects need to be further addressed. Fundamental research is thus needed to improve the quantification of the differential release/retention phenomenon, in order to more accurately estimate the recoverable amount of in situ hydrocarbons.

The structure of kerogen is widely believed to have significant impact on the differential release effect of shale reservoirs [12,13]. Modified from [14], Fig. 1A shows the morphological characterization of a reconstructed kerogen material. Fig. 1B is a scanning electron

microscope (TEM) photo of a Barnett shale example containing both organic matters and inorganic matters. According to these two sub-plots, kerogen has a hierarchical pore structure. The radius of aperture ranges from about 1 nm to a few dozens of nanometers. Moreover, certain larger (bulk) pores are isolated. This maybe because the hydrocarbon molecules in shale reservoirs haven't gone through the 'primary migration' process [2,15]. As such, during the primary depletion process, the hydrocarbon molecules within the isolated (dead-end) larger pores need to flow through narrower pores (pore throat), resulting in the retention of the hydrocarbons. Hence, a conceptual model of this process can be formulated as follows: during the hydraulic fracturing process, the shale rock is cracked and the micro-cracks within the rock are enhanced. The micro-fractures, the inorganic pores and connected bulk pores serve as the main flow path during the depletion [16]. The rest of the kerogen, including the dead-end pores, serves as a hydrocarbon 'source'. In this work, we are particularly interested in the transport dynamics of the hydrocarbon molecules between the dead-end pores and the bulk pores, as shown in Fig. 1C. Previously, Zhu et al. [5] studied the selective release of hydrocarbon mixtures in Niobrara shale rocks and concluded that the nano pore system has considerable hindering

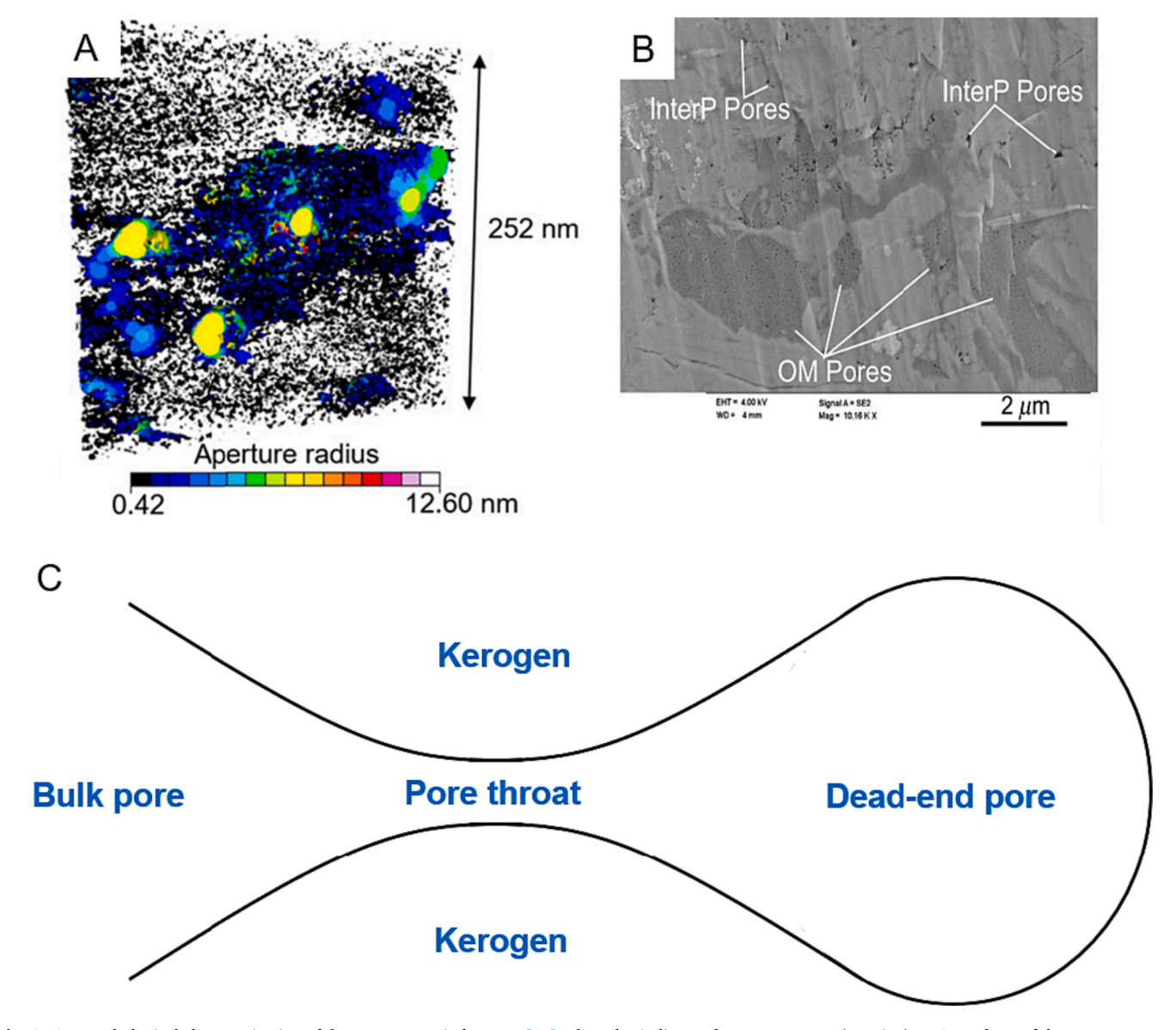


Fig. 1. A: Morphological characterization of the pore system in kerogen [14]. The color indicates the pore aperture (opening). B: SEM photo of the pore structure of shale [18]. C: Conceptual model of a bulk pore and a dead-end pore connected by a pore throat win the kerogen.

impact on the heavy components of in situ hydrocarbon. Moreover, the hindering effect can be partially mitigated by the injection of  $\mathrm{CO}_2$ . A limitation of Zhu et al. [5]'s work is that the structure of the nano pore is not explicitly modeled, leading to the lack of quantitative analysis. Hong et al. [17] investigated the migration of hydrocarbon mixtures through a kerogen pore throat and found out that the heavier components may block the throat causing differential retention of different components.

To increase the cumulative production, the enhanced oil recovery (EOR) techniques, which have achieved great success in conventional reservoirs [19,20], have been extended to unconventional reservoirs. According to field scale observations, gas huff-n-puff is among the few EOR techniques that are proved to be profitable in unconventional reservoirs. In a gas huff-n-puff operation, working gas, such as lightweighted hydrocarbon, CO2 and flue gas, is cyclically injected (huff) into and produced (puff) from the reservoir. In between the huff and the puff operation, the well is shut down for a period of time, in order to allow the injected gas to further infiltrates the reservoir, known as the 'soaking' operation. During the huff-n-puff process, the in situ reservoir oil is mobilized and the production rate is enhanced. Fig. 2 presents a conceptual example of the variation of production rate and the bottom hole pressure (BHP) of a huff-n-puff cycle following a primary depletion stage. It has been observed [17] that the rock properties and the type of injected gases have substantial impacts on the EOR performance in the shale and tight reservoirs. In this work, we aim to investigate the gas EOR process at the pore scale by considering the rock-fluid interaction as well as the rock heterogeneity. We have conducted molecular dynamics (MD) studies to enhance the understandings of the condensate trapping mechanism within the kerogen. Moreover, we have investigated the performance of different injection gases on the improvement of trapped hydrocarbons. Our study differs from previous ones in that we aim to study the transport dynamics of hydrocarbon mixtures through a pore throat. The novelty of our work is that we have further illustrated the importance of the compositional change on the differential release effect. We are arguably the first to study the condensate trapping induced by differential retention of the pore throat. Through the numerical analysis, we have obtained a clearer view of the trapping mechanism induced by different portions of the inhomogeneous porosity system. In particular, we find that significant amounts of lighter components are trapped in dead-end pores and can be potentially recovered by gas huffn-puff. We highlight that the compositional path plays an important role in the capillary condensate trapping process. We have also compared the performance of different working gases for huff-n-puff, and found that heavier injecting gases are more likely to remove the residual hydrocarbons. We believe such findings will improve the estimation of recoverable in situ oil as well as the selection of working gases of gas EOR. In shale oil reservoirs.

This paper is organized as follows. In Section 2, we describe the MD model setup as well as the procedures of the simulation of the primary depletion and gas huff-n-puff. In Section 3, we present the results and analysis of the MD simulation. This paper is concluded by Section 4.

#### 2. Methodology

In this section, we describe the methodology used in this work, including the setup of the MD system and the steps of the simulation of the primary depletion as well as the gas huff-n-puff process.

## 2.1. Molecular dynamic system setup

To mimic the pore structure described in Section 1, we set up a dual-bath MD system as shown in Fig. 3A. The left and right bath represents the bulk pore and the dead-end pore, respectively. The length of the MD system is 17.4 nm and 11.6 nm along the y and z direction, respectively. The length of the right bath is set to be 12 nm along the x direction. As reported by [21,22], when the pore aperture is above 10 nm, the nano confinement effect is no longer significant.

We set the boundaries along y and z direction of the two baths to be periodic, and set two constraining atom walls at the two-ends of the

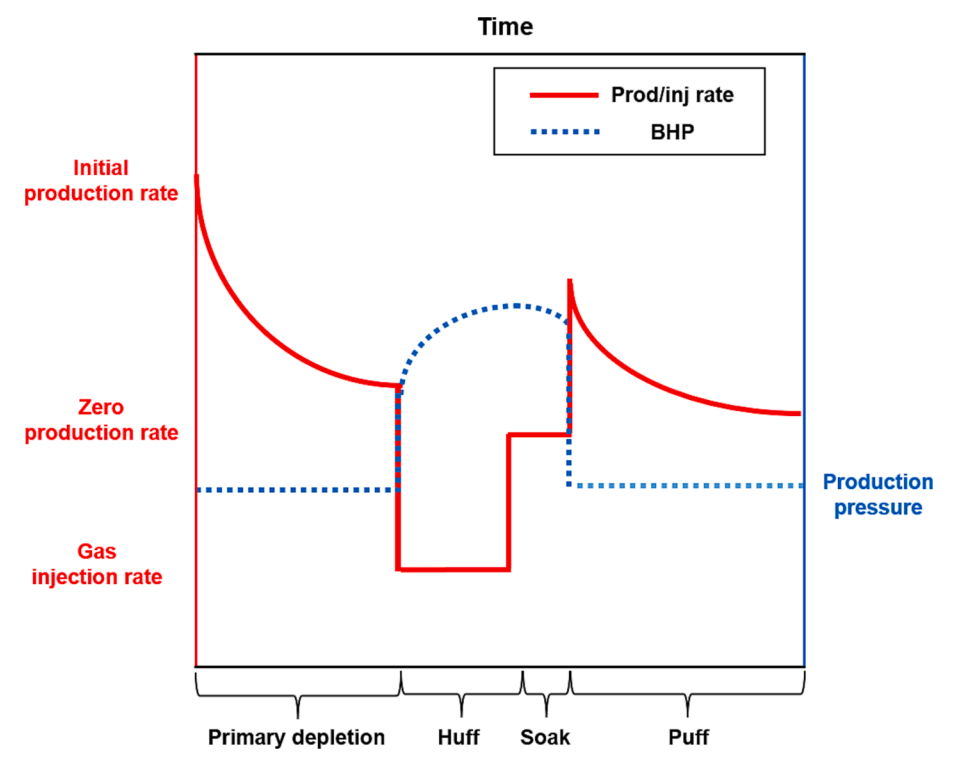


Fig. 2. A conceptual example of the variation of injection/production rate and the bottom hole pressure of a gas huff-n-puff operation following the primary depletion operation. Solid blue line: curve injection and production rate. Positive value corresponds to production. Red dash line: bottom hole pressure. (For interpretation of the references to color in this figure legend, the reader is referred to the web version of this article.)

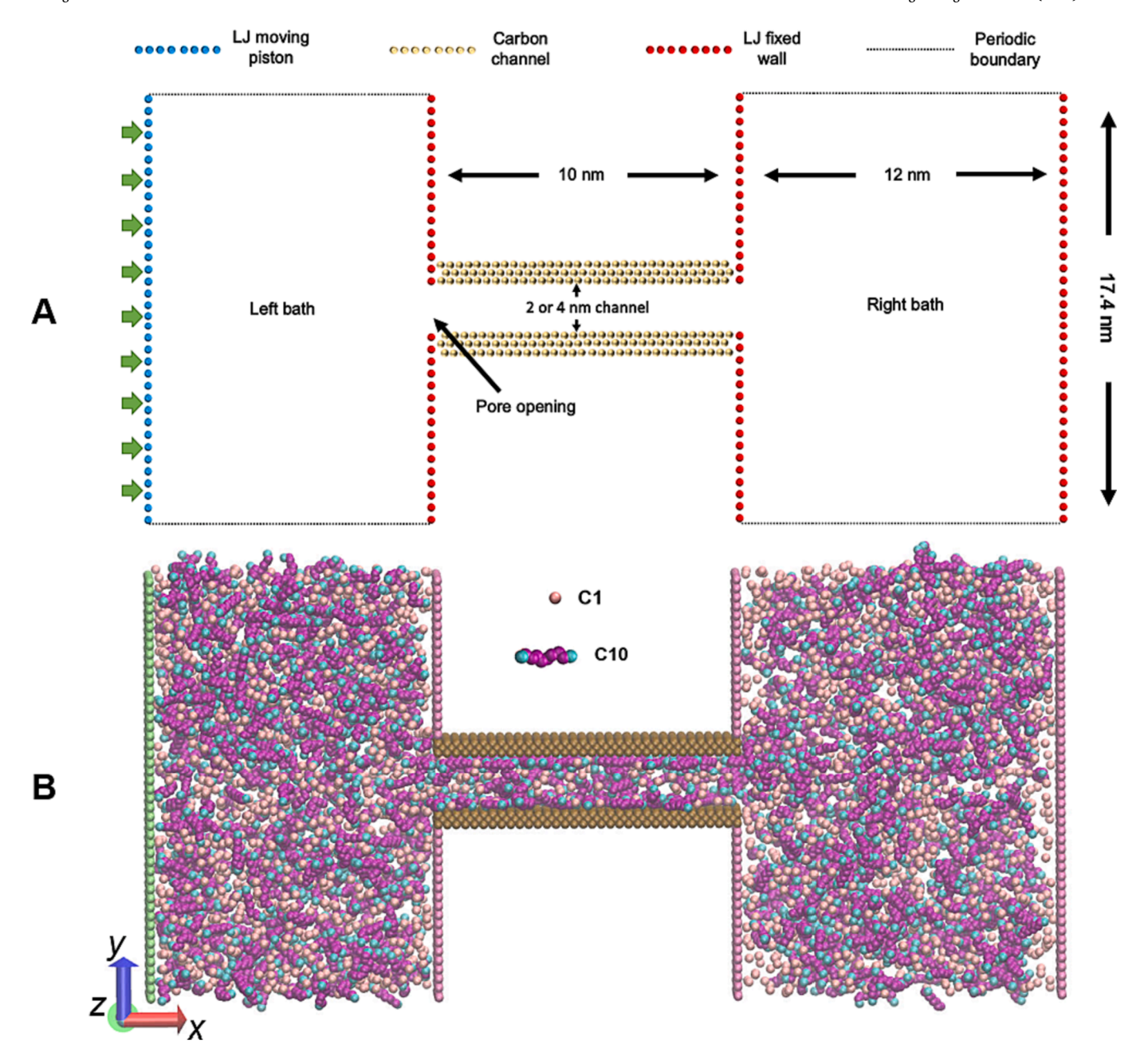


Fig. 3. A: configuration of the MD system. The green arrows indicate the pressure applied on the piston wall. B: status of the MD system at the end of the pre-equilibrium step. (For interpretation of the references to color in this figure legend, the reader is referred to the web version of this article.)

system along the x direction. The constraining wall for the left bath is a moving piston, to control the pressure in the system, while the constraining wall for the right bath is fixed. The volume of the left bath can thus change during simulation. We assume that the left bath (bulk pore) is connected with either hydraulic fractures or micro-cracks, so that its pressure changes quickly to the bottom hole pressure.

The two baths are connected by a nano channel to mimic the pore throat in the kerogen. We adopt a slit-shaped nano channel made of two parallel slabs because slit pores are pervasively found in shale reservoirs (see [23,24]). The width of the nano channel is either 2 nm or 4 nm, which allows us to investigate the impact of the channel width on the transport mechanism. The length of the nano channel is set to 10 nm. While this length is much shorter than those in real reservoirs and thus leads to fast gas release kinetics, it does not affect many essential features of gas release, e.g., differential release of different hydrocarbons during primary depletion, heterogeneous distribution of different

components in pores, and the evolution of gas-oil ratio and its modulation by gas injection. This is because, as we shall see below, these features are governed by the *thermodynamics* of gas behavior in nanopores, which depends strongly on gas-wall interactions in direction normal to pore walls (and thus the pore width) only. Once the pore length becomes considerably longer than the range of fluid molecule-pore wall interactions (typically a few nanometers), the thermodynamic aspect of gas behavior in nanopores becomes insensitive to the pore length.

The nano-channel is modeled as two parallel walls. There exist many different approaches for modeling the pore walls, e.g., they can be modeled using kerogens with full molecular details [8,9,11], using graphene/graphite sheets [23,24], using slab of atoms cut from crystal lattices [25], or using implicit walls that model the fluid-wall interactions only in directions normal to the pore walls [10]. Using realistic kerogen is desirable but will incur substantial computation costs,

particularly because our pore is long (10 nm). We therefore choose pore walls built from crystal lattices because such as coarse-grained description of pore walls still allows the adsorption of gas molecules on the pore wall, which governs the phenomena studied in our work, to be simulated faithfully with modest cost [25]. Each slab consists of two layers of atoms that are packed as a Face-Centered Cubic (FCC-111) lattice. The lattice constant is set to be 0.54 nm [25]. The relatively low density of wall atoms compared to other common choices of model kerogen pore wall (e.g., those made of graphite/graphene) helps further reduce the computational cost. As shown previously, by judiciously selecting the Lennard-Jones parameters for fluid-wall interactions, still allow the molecular adsorption on pore walls to be modeled well [25–27].

Except the walls in the nano channel, all other walls in the MD system are used as boundaries without adsorption or confinement effect. We call these walls as 'LJ walls' and use atoms with the Lennard-Jones (LJ) 12-6 potential to model them, as shown in Eq. (1).

$$\phi_{ij} = 4\varepsilon_{ij} \left[ \left( \frac{\sigma_{ij}}{r} \right)^{12} - \left( \frac{\sigma_{ij}}{r} \right)^{6} \right]$$
 (1)

In the above equation,  $\phi_{ij}$  is the LJ potential between molecule i and j. r is the distance between the two molecules.  $\varepsilon_{ij}$  and  $\sigma_{ij}$  are calculated by the Lorentz-Berthelot rule, as below

$$\varepsilon_{ij} = \sqrt{\varepsilon_i \varepsilon_j} \tag{2}$$

$$\sigma_{ij} = \frac{\sigma_i + \sigma_j}{2} \tag{3}$$

In the above equations,  $\varepsilon$  and  $\sigma$  is the potential well depth and the distance at which the energy is zero, respectively.

As pointed out by Hong et al. [17], the release of hydrocarbon from kerogens to the inorganic pores also has differential retention effect. As such, the conclusion drawn from the present work can be extended to the kerogen case, for the investigation of the release behavior of hydrocarbon molecules from the organic matter (OM) to the inorganic matter (IM).

In order to investigate the compositional effect on the transport mechanism, we use a light component (methane) and a heavy component (decane) to represent the in situ oil. The reason we choose these two components is that we know beforehand that most methane molecules exists in the gas phase while most decane molecules exist in the liquid phase in the nano pore system, which makes our analysis on the phase behavior of the binary mixture more convenient. The hydrocarbon are modeled by the TraPPE force field [28]. In the TraPPE force field, each carbon atom, along with its bonded hydrogen atoms, in a nalkane molecule is modeled as a coarse spherical pseudo-atom. It has been shown by numerous works in the literature that TraPPE force field is of reasonable accuracy and sound flexibility in modeling hydrocarbon flows [25,29,30]. TraPPE force field is also based on LJ 12-6 potential, as shown in Eq. (1). The parameters of the LJ potential for all atoms used in this work are listed in Table 1, where  $k_{\text{B}}$  refers to the Boltzmann constant. Note that the  $\sigma$  parameter of nano channel wall atoms was selected so that fluid molecules do not leak through the pore walls. The  $\varepsilon$ parameter, i.e., the depth of the Lennard-Jones potential well, was essentially taken as those in Ref. [25]. As pointed out in that paper, the parameters (and consequently, the fluid-wall interactions) leads to

Table 1
The parameters used for TraPPE force field for atom–atom interactions.

Atom group	$\sigma$ (nm)	$\varepsilon/k_B(\mathbf{K})$
CH4	0.3730	148.0
CH3	0.3750	98.0
CH2	0.3950	46.7
Atoms of nano walls	0.5763	297.0
Atoms of LJ walls	0.0050	297.0

hydrocarbon adsorption on pore walls similar to those observed in organic nanopores.

Because of the surface preference of hydrocarbon molecules [6] as well as the confinement effect induced by the nano channel walls [31], the distribution of hydrocarbon components within the MD system is not uniform. The fraction of lighter components tends to be higher in the bath chambers, while heavier components tend to cumulate inside the nano channel. The split of hydrocarbon components inside a system with both bath pores and nano channel can be calculated by the confined equation of state. We use a confined equation of state [32] that is based on global minimization of free energies to estimate the initial distribution of components in the system. Such a calculation reduces the time for the system to get equilibrium, as will be discussed in the next section.

The MD simulation is conducted by the LAMMPS software [33], which is a widely-adopted MD simulation platform. During the MD simulation, the system temperature is maintained to be 353.15 K (80  $^{\circ}$  C) using the Nose-Hoover thermostat [34]. The cut-off radius is set to be 10 nm, and the time step of the simulation is 1 fs per step. We use NVT ensemble in the simulation, and the pressure of the system is controlled by the moving piston wall. Before the dynamic simulation of the atoms, we first minimize the energy of the system using the 'minimize' command in LAMMPS. The energy minimization is run for a maximum of 1000 steps with a tolerance 1e-4. Each set of simulation is conducted by three times with different initial configurations to reduce the random effect.

## 2.2. Simulation of primary depletion

The MD simulation of the primary depletion process consists of two steps. In the first step, we randomly place hydrocarbon molecules using the Packmol program [35] in the system and apply a constant force on the moving piston, to build up the system pressure to P1 (35 MPa in this case). In this work we use 8000 methane molecules and 4000 decane molecules, so that the overall C1-C10 ratio is 2:1. The initial number of hydrocarbon molecules in each part of the system is estimated by a confined equation of state, as described in the previous section. We run the simulation by 10 ns for the system to self-equilibrate. We monitor the position of the moving piston and the density distribution of the hydrocarbons. After about 2 ns, the fluctuation of the above status indicators is below 5 %, indicating that the system is in thermodynamical equilibrium. A snapshot of the MD system at the end of the preequilibrium step is shown in Fig. 1B. Then as the second step, we reduce the pressure on the moving piston to P2 (6 MPa in this case) and let the molecules inside the nano-channel as well as the right bath to release. We monitor the number and composition of the released hydrocarbon molecules at the channel opening, to study the differential release effect. Moreover, we track the change of the composition in the nano channel and the right bath, to investigate the trapping mechanism induced by the nano channel. A conceptual flowchart of this procedure is shown in Fig. 4.

## 2.3. Simulation of gas huff-n-puff

The MD simulation of the gas huff-n-puff operation consists of three steps. The configuration of the walls used in the gas huff-n-puff simulation is the same as that used in the primary depletion simulation. In the first step of the gas huff-n-puff simulation, shown in Fig. 5A, we fill the nano channel and the right bath based on the hydrocarbon densities in them at the end of the primary depletion step, as a mimic of the reservoir condition at the start of the huff-n-puff. We fill the left bath with methane (C1) or propane (C3) molecules as the injection gas. We use a 'ghost wall' to separate the left bath with the rest of the system and apply pressure P3 on the left piston to equilibrate the system. In this work, P3 is set to be 40 MPa as the bottom hole pressure at the huff step. This step is run for 10 ns. In the second step (huff), shown in Fig. 5B, the ghost wall atoms are removed using the 'delete' command in LAMMPS and the

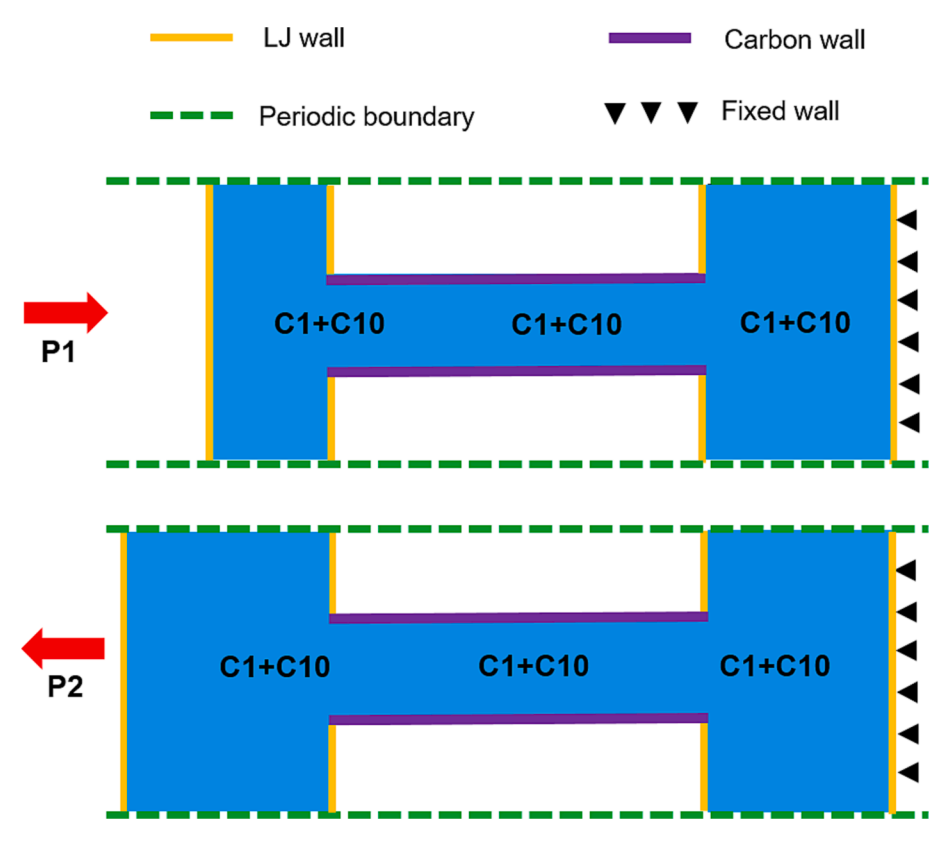


Fig. 4. Conceptual model of the workflow of the primary depletion simulation. upper: pressure build-up and pre-equilibrium; lower: depletion. The red arrows indicate the direction of piston movement. (For interpretation of the references to color in this figure legend, the reader is referred to the web version of this article.)

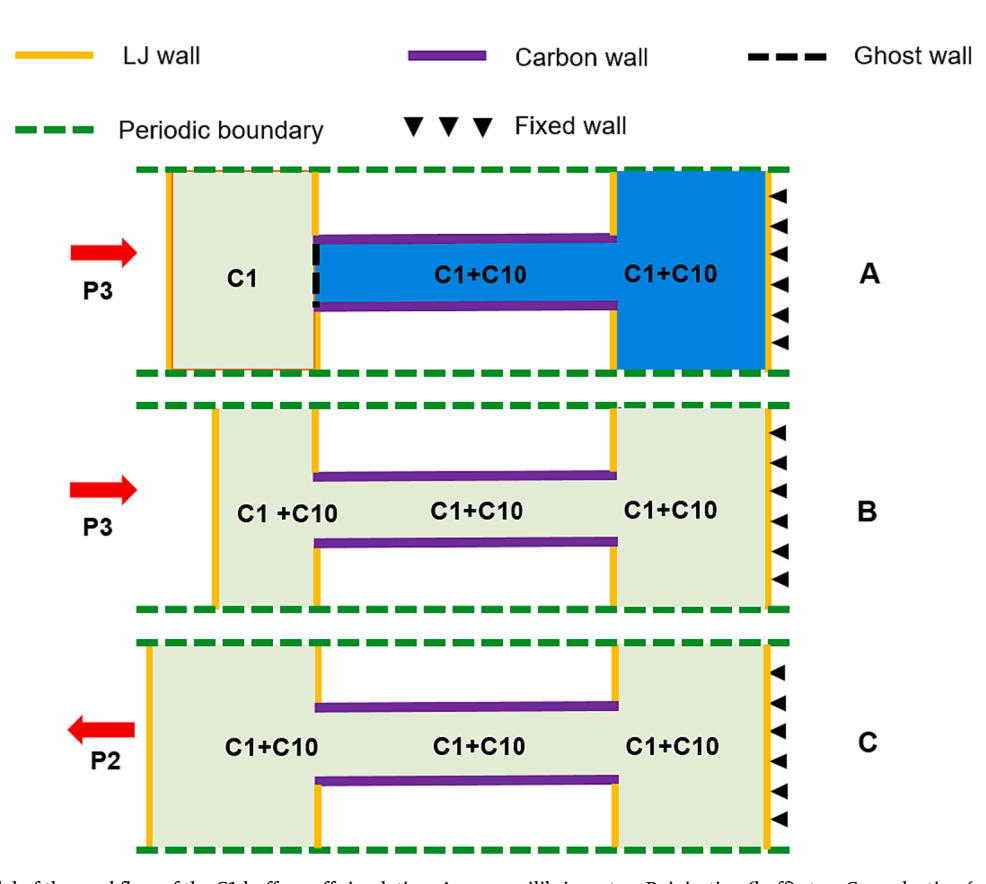


Fig. 5. Conceptual model of the workflow of the C1 huff-n-puff simulation. A: pre-equilibrium step; B: injection (huff) step; C: production (puff) step. The legends in this figure are the same as those in Fig. 4.

gas hydrocarbon molecules flow into the nano channel. This step is run for 2 ns. In the third step (puff), shown in Fig. 5C, the pressure on the left piston is reduced to P2 again to deplete the system.

#### 3. Results

#### 3.1. MD results of primary depletion

As the results, Fig. 6A shows the variation of methane (C1) to decane (C10) ratio within the right bath. According to the figure, the percentage of the lighter component in the right bath significantly increases as the pressure decreases. Fig. 6A compares the ratio of C1 to C10 molecules that are released from the channel opening. The releasing ratio is analogous to the gas-oil ratio (GOR) in reservoir production. According to the results, the releasing ratio at the beginning of the depletion is higher than 2, which is the in situ C1-C10 ratio, indicating the occurrence of the differential release effect. The differential release effect is because the lighter components have relatively less adherence to the rock surface. Hence, C1 has less retention in the nano channel and releases faster compared to C10. The releasing ratio declines over time, as the amount of C1 decreases in the nano channel. The differential release effect is more obvious in the 2 nm channel case, because narrower channels have stronger molecule-wall interactions. Fig. 6B and C shows

the C1-C10 ratio in the nano channel and in the right bath, respectively. The ratio decreases in the nano channel while increases in the right bath. For the right bath, C10 enters the nano channel faster than C1, because of the preferential adsorption effect in the channel, causing the hydrocarbon mixture in the bath to be lighter. Since the nano channel has faster methane releasing rate at the left opening and higher decane entering rate (from the right bath), the methane to decane ratio in its nano channel rapidly decreases, causing the fluid inside the channel to be significantly denser. In Fig. 6D we plot out the pressure variation in the right bath. Particularly, we compare the outlet pressure in the right bath with that in the left bath, which is analogous to the bottom hole pressure (BHP) during reservoir recovery. It can be seen from Fig. 6D that the right bath pressure declines over time. The eventual value of the pressure is however higher that the outlet pressure. The 2 nm case has relatively higher eventual pressure than the 4 nm case. This phenomenon indicates that the hydrocarbon mixture in the right bath changes to a gas-like phase as it becomes lighter. The phase change leads to the occurrence of capillary pressure. As such the pressure in the right bath is above the outlet pressure. In the bulk pores, the capillary pressure is inversely proportional to the pore diameter, according to the Young-Laplace equation. In our case, the eventual pressure in the dead-end pore of the 2 nm system is also significantly higher than the outlet pressure. These results indicate that considerable quantities of lighter

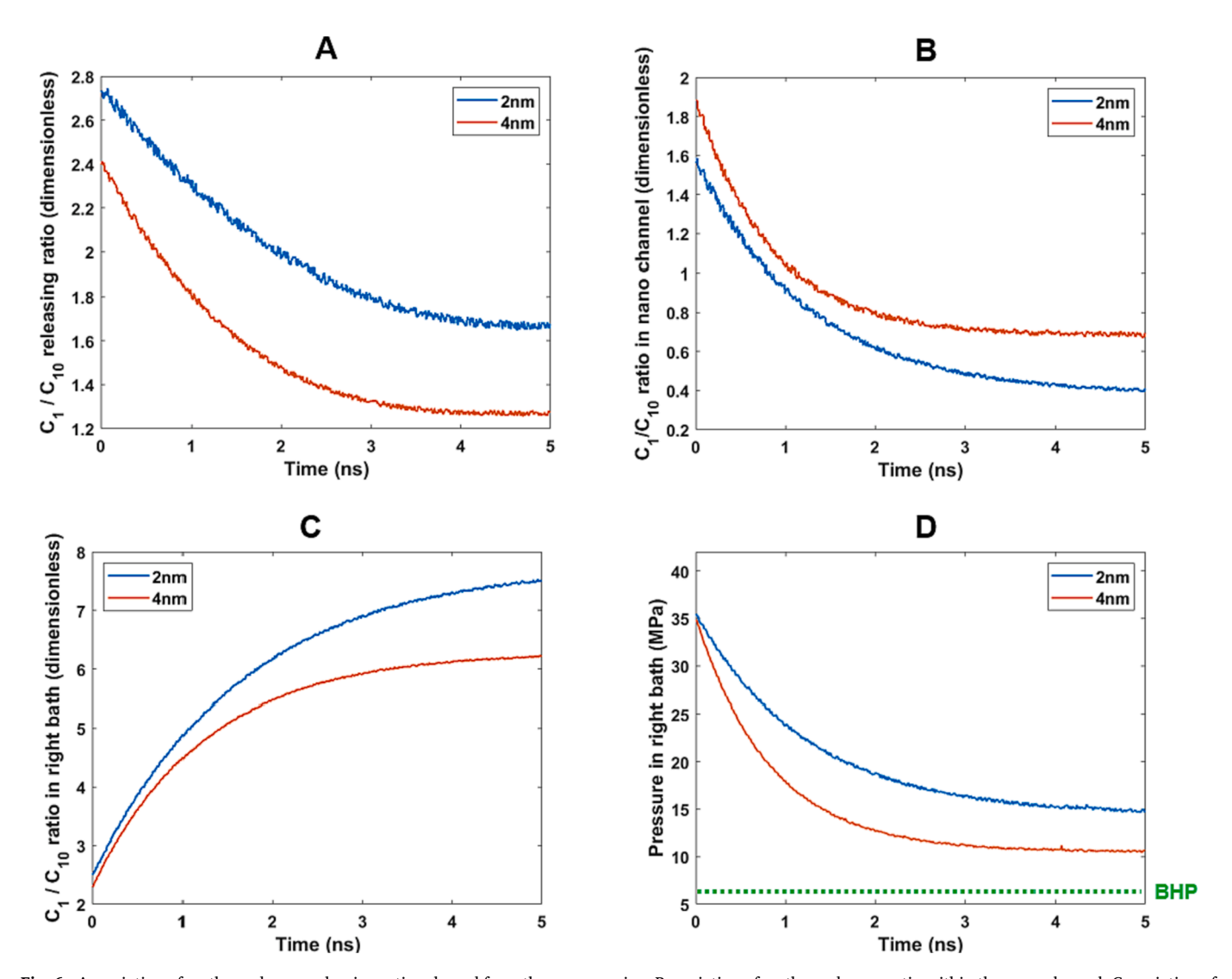


Fig. 6. A: variation of methane-decane releasing ratio released from the pore opening. B: variation of methane-decane ratio within the nano channel. C: variation of methane-decane ratio in the right bath. D: variation of pressure within the right bath.

components and heavier components are trapped in the right bath and in the nano channel, respectively.

The differential release is further visualized in Fig. 7. In Fig. 7a and b, we compare the mole density profile of C1 and C10 in the 2 nm case before and after the primary depletion. From the figures, it can be seen that both hydrocarbons form two adsorption layers, which is consistent with the observations in [21]. After the depletion, the relative fraction of C1 in the channel decreases, particularly in the region in the middle of the nano channel. We calculate the mole flux ratio between C1 and C10, following the approach described in [6], as shown in Fig. 7c. The result implies that C1 molecules flow much faster than C10 in the middle of nano channel. The mole flux ratio is higher than the in situ mole fraction ratio, resulting in the differential release phenomenon shown in Fig. 6.

To further illustrate the trapping process, we plot the 3D snapshots of the MD system in Fig. 8. The distribution profiles of hydrocarbons in the MD system before and after the primary depletion are shown in the left and right of Fig. 8, respectively. According to the 3D plots, the decane molecules (represented by purple chains) accumulate in the nano channel after the primary depletion. Meanwhile the fraction of methane molecules (represented by brown dots) significantly increases and the hydrocarbon mixture in the right bath becomes sparser as the system pressure drops. The accumulated heavier components in the nano channel then form a liquid-like phase, which reduces the further release of hydrocarbons from the gas-like phase in the right bath. Such visualization is clear evidence of the existence of the capillary condensate trapping mechanism. Fig. 9 is a phase diagram of C1-C10 mixtures. The x axis and y axis of the figure is the system pressure and the C1 mole fraction, respectively. The color indicates the fraction of gas phase in the system. The diagram is calculated using an in-house flash calculator based on the Peng-Robinson equation of state (PR-EOS) [36]. We plot out the phase condition of the right bath and the nano channel in the phase diagram, as shown by the stars and the crosses, respectively. Since there is no reliable approach to directly calculate the pressure inside the nano channel due to the wall impacts, we use the average pressure

between the left and right bath to represent the pressure inside the channel. As can be seen from the figure, the hydrocarbons in the two regions of the system follow different compositional paths during the primary depletion process. The hydrocarbons in the right bath change from the liquid-like phase to the gas-like phase, while the hydrocarbons in the nano channel remain to be the liquid-like phase. Since heavier components tend to accumulate within the nano channel, their viscosity increases, which prevents further release of lighter components in the right bath. This result is our main finding for the explanation of the capillary trapping mechanism. Based on the above results and analysis, we have developed a systematic model of capillary condensation trapping in the nano channel that includes competitive adsorption and differential retention effects, as shown in Fig. 10.

In the previous works, the trapping mechanism is mainly attributed to the capillary pressure induced by the heterogeneity of the rock. In this work, we have shown that the trapping mechanism also includes the condensation of heavier components, which is a 'compositional effect'. As such, the above-mentioned mechanism can be named as 'capillary condensation trapping'. We, arguably for the first time, quantitatively investigate it while highlighting the importance of the compositional path.

Moreover, the results of the 2 nm case has relative larger fluctuations compared to the 4 nm case, which is consistent with our observations in gas flow cases [6]. This phenomenon is potentially due to the diffusion effect [39]. As the channel becomes narrower, there are more molecular-wall interactions and the diffusion, including bulk and surface diffusion, becomes more dominant, resulting in more fluctuations in the releasing ratio.

## 3.2. Results of huff-n-puff simulation

In this sub-section, we report our MD results and analysis of the gas huff-n-puff in the depleted system resulted from section 3.2. Fig. 11 compares the snapshots of methane and propane injection at the 0.7 ns

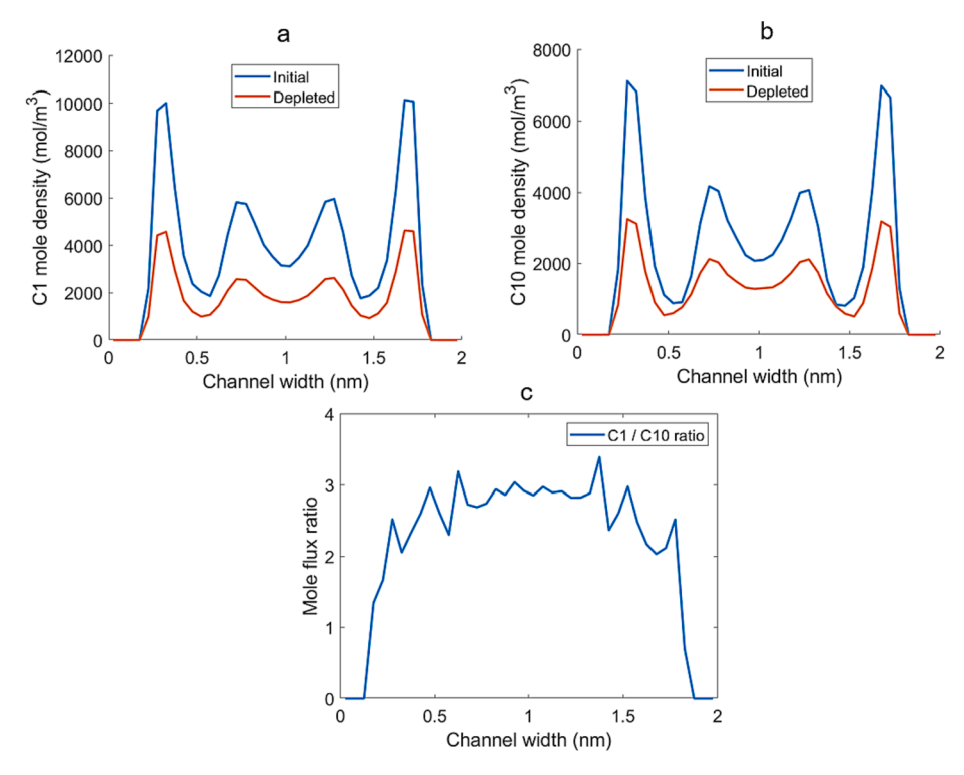
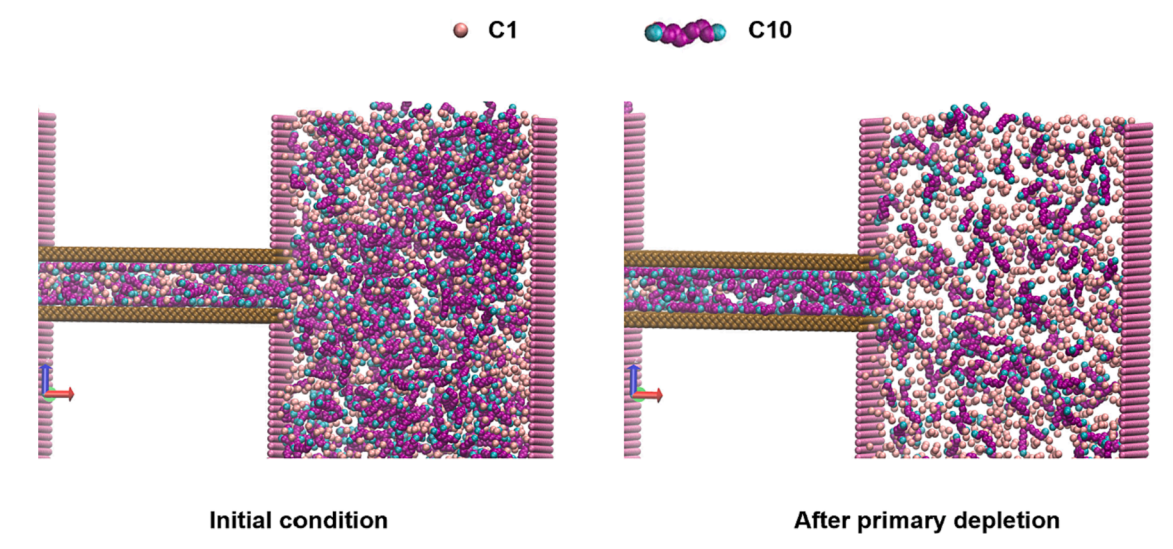
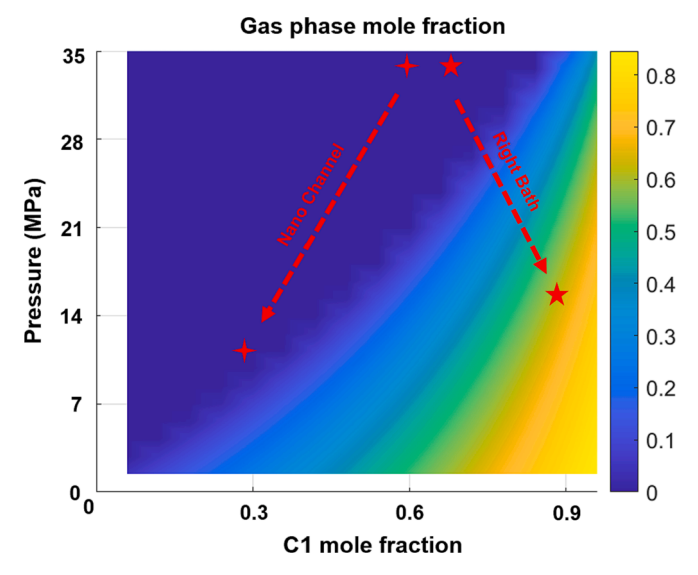


Fig. 7. A C1 adsorption profile of the 2 nm case before and after the primary depletion; B C10 adsorption profile of the 2 nm case before and after the primary depletion; c mole flux ratio between C1 and C10 at the beginning of the depletion. There is a 0.1 nm wide no-molecule zone in the vicinity of the channel walls. The mole flux is set to be zero in this region.



**Fig. 8.** Left: initial condition of the 2 nm nano channel and the right bath with C1-C10 ratio being 2:1 in the system. Right: the distribution of C1 and C10 in the system after the primary depletion. The brown dots denote C1 molecules, while the purple chains with blue ends denote the C10 molecules. (For interpretation of the references to color in this figure legend, the reader is referred to the web version of this article.)



**Fig. 9.** Compositional path of hydrocarbon mixtures in the nano channel and in the right bath. The four-pointed star refers to the nano channel, while the pentagram refers to the right bath.

of the simulation. From the figure, two phenomena can be observed. On one hand, methane molecules mainly flow through the nano channel in the middle, leaving a considerable number of decane molecules adsorbed on the pore wall. Propane molecules, however, demonstrate stronger competitive adsorption capability and sweep the nano channel more thoroughly than methane. This can be clearly seen at the opening between the nano channel and the right bath (denoted by black arrows in Fig. 11). In the propane injection case, decane molecules are continuously displaced out of the nano channel into the right bath. The root cause of the difference in the displacement behavior between the two types of molecules mainly lies in their competitive adsorption capability. Methane molecules have much lower adsorption capability and lower surface diffusion capability, compared to the in situ decane-rich hydrocarbons, resulting in their 'channeling' displacement behavior. A similar phenomenon has been observed when methane was injected into a slit-shaped calcite nanopore to recover the decane in it [40]. On the other hand, methane flows faster than propane into the nano channel. As

methane molecules break through into the right bath, the front of propane molecules is still within the channel. This is mainly due to the relative lower viscosity and higher bulk diffusivity of the methane-decane mixture. Such a phenomenon implies that propane injection requires a relative longer soaking time for the working fluids to fully infiltrate the hydrocarbon-saturated pore.

Fig. 12 shows the variation of C10 recovery ratio during the primary depletion and after the gas injection. We measure the number of C10 molecules in the nano channel and the right bath and divide the value by the initial number of C10 molecules in the system. The left sub-plot in Fig. 12 compares the C10 recovery ratio during the primary depletion stage. As can be seen from the figure, the 4 nm case has higher recovery ratio than the 2 nm case, because of the difference in the capillary trapping capability that is discussed in the previous section. The eventual recovery ratio of C10 in the 2 nm case is about 55 %. The remaining C10 molecules mainly exist in the nano channel. We then use the 2 nm case to investigate the recovery capability of C1 and C3 gas, as shown in the right of Fig. 12. According to the figure, the recovery ratio of the C1 case increases quickly at the beginning but then becomes flat, compared to the C3 case. The additional C10 recovery owing to C1 and C3 is about 4 % and 9 %, respectively. This is because of the following reasons. Once the in situ oil is mixed with the injected C1 gas, its viscosity is lower than that of the C3 case. As such, the hydrocarbon molecules in the C1 case flow relative faster. Moreover, as shown in Fig. 11, during the huff stage C1 breaks through the hydrocarbons in the nano channel in a channeling manner, leaving a relatively larger amount of C10 molecules in the channel. Hence, during the puff stage, the remaining C10 in the nano channel will flow out of the opening relatively faster. C3 molecules, on the other hand, sweep the C10 molecules more thoroughly in the huff stage. It then takes longer for the C10 molecules to flow back to the pore opening during the puff stage. However, since C1 has weaker competitive adsorption capability compared to C3, its eventual recovery ratio is lower. Such findings are consistent with field observations that heavier injected gases in general have better recovery capabilities. The C10 mole density profile in the nano channel before and after the gas injection is shown in Fig. 13, which further shows that C3 has superior competitive adsorption capabilities to remove C10 compared to C1. From the economical perspective, C3 is more expensive than C1 as working gases. As such, an optimization strategy that integrates technical and economic considerations needs to be developed in order to screen the optimal working gases, which is our ongoing work. It should be pointed out that, in this work the overall recovery efficiency of shale and tight reservoirs

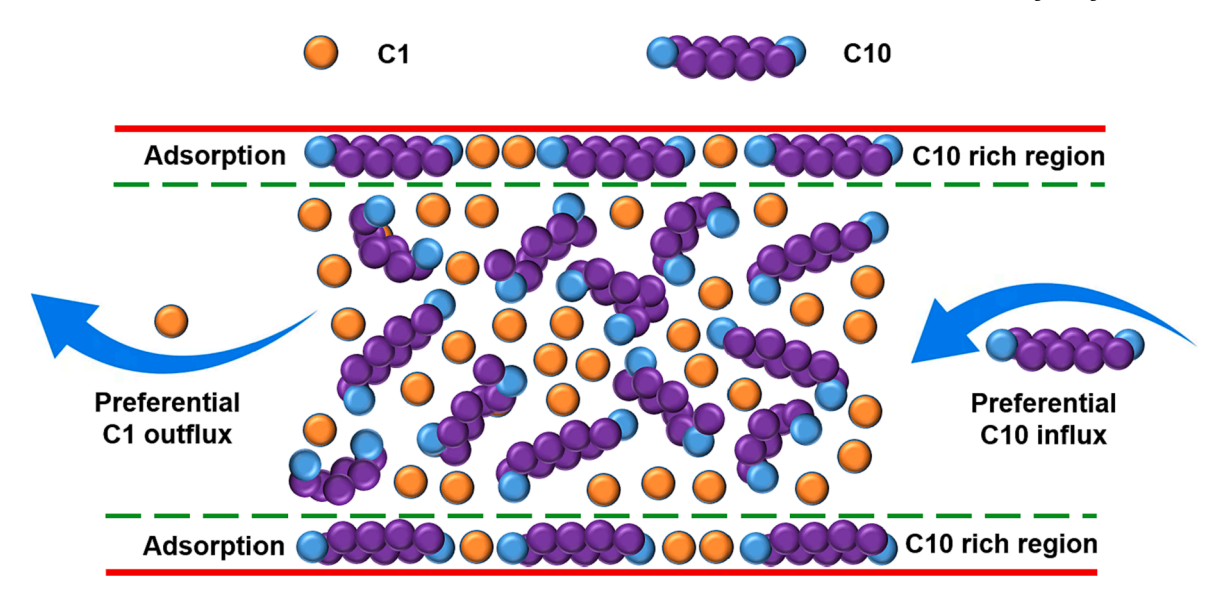


Fig. 10. Conceptual model of the capillary condensate mechanism.

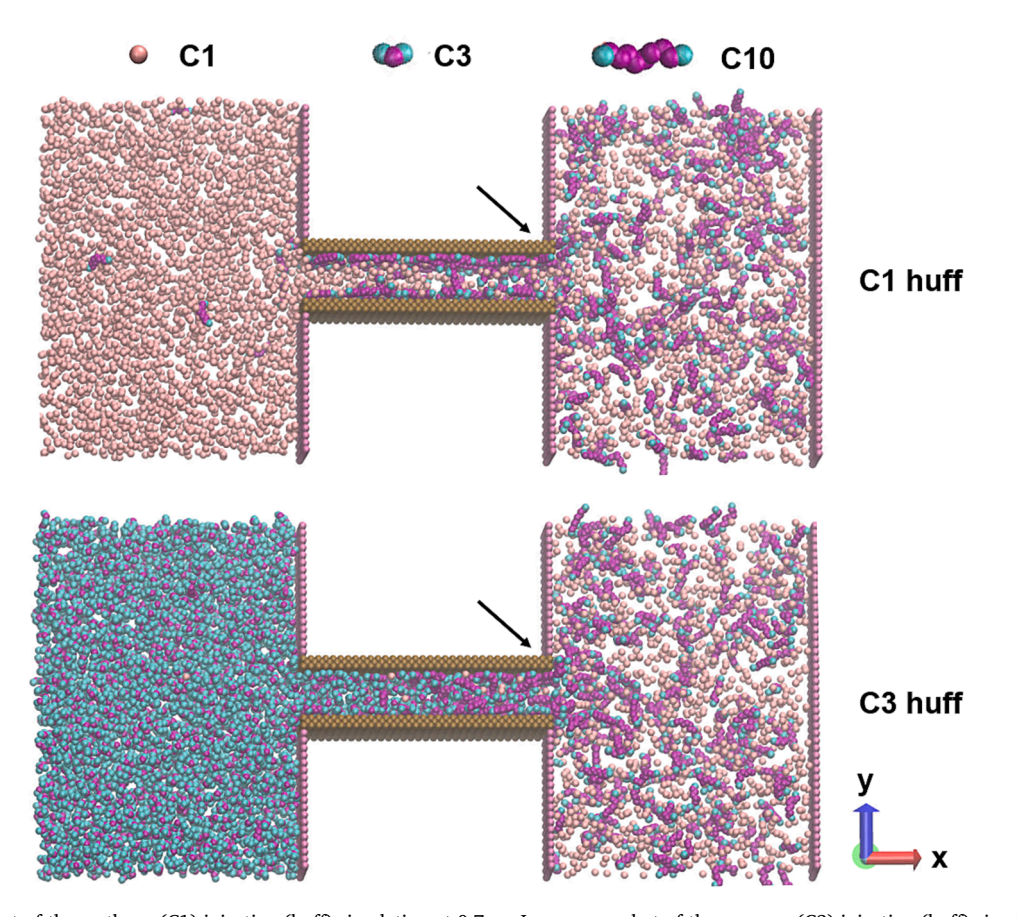


Fig. 11. Upper: snapshot of the methane (C1) injection (huff) simulation at 0.7 ns. Lower: snapshot of the propane (C3) injection (huff) simulation at 0.7 ns. The black arrows point to where decane molecules are pushed back to the right bath.

is up to about 70 %, according to the MD results, which are distinct with the field observations ( $<\!5\%\sim10$ %). This is because in this work only one single nano pore is taken into consideration. In practice, the pressure drawdown only propagates a few meters away from the hydraulic fracture, due to the low permeability of the unstimulated rocks. The limited pressure-swept volume leads to the low recovery efficiency in reality. In this way, our work does not contradict field observations. Indeed it provides insights to the EOR operations in practice.

#### 4. Conclusion and summary

In this work, we have comprehensively investigated the primary depletion and the gas huff-n-puff process in shale reservoirs using a novel MD system. We have particularly analyzed the trapping mechanism induced by compositional condensation.

The findings of this work are as below:

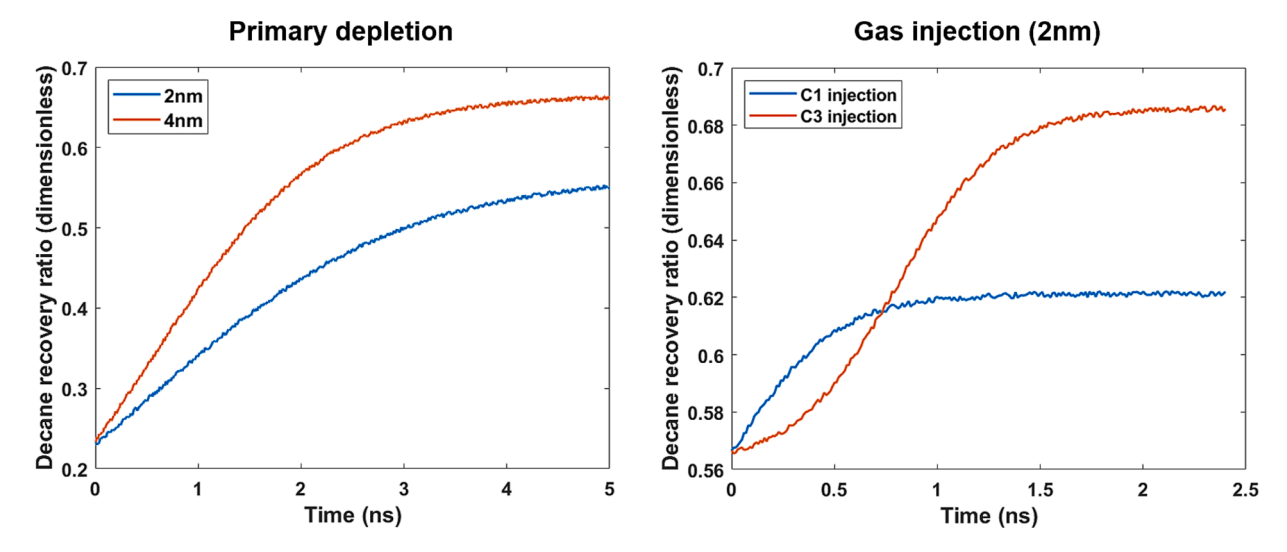


Fig. 12. Left: the variation of recovery ratio of C10 during the primary depletion. Right: comparison of the recovery ratio variation with C1 and C3 injection for the 2 nm case.

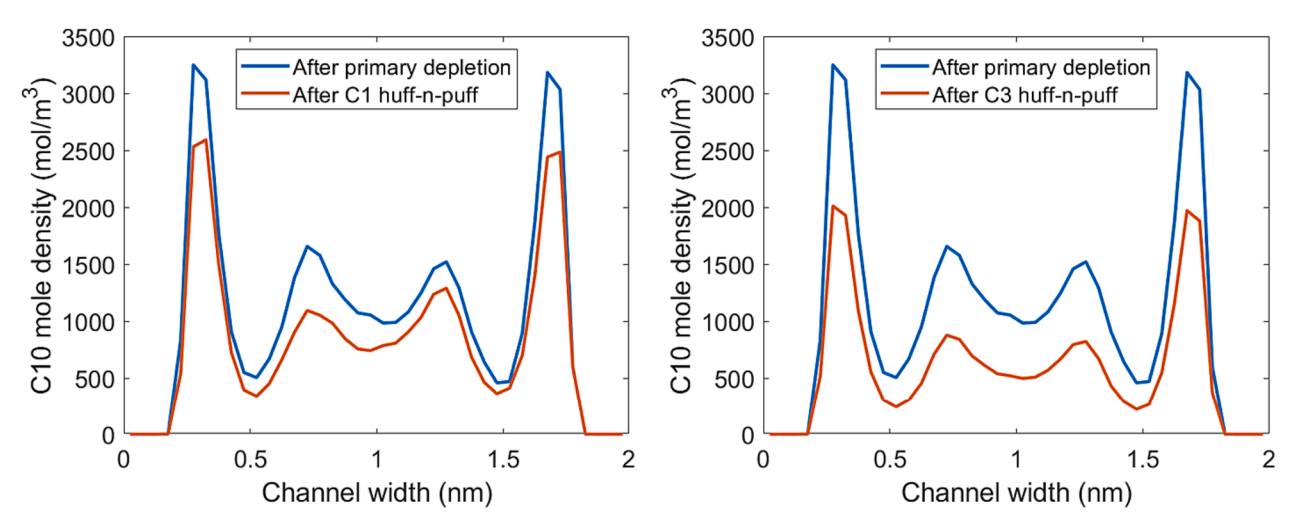


Fig. 13. The C10 mole density profile in the nano channel after the gas huff-n-puff simulation. Left: C1 huff-n-puff. Right: C3 huff-n-puff.

- Significant amounts of heavier and lighter components are trapped in the narrow channel and the dead-end pores in the kerogen due to the capillary condensation trapping mechanism after the primary depletion.
- The capillary condensation trapping mechanism is resulted from the accumulation of liquid-forming heavier components, which implies that compositional effects as well as nano confinement effects are important in the development of shale and tight reservoirs.
- Gas huff-n-puff effectively improves the recovery of the trapped hydrocarbon molecules. Heavier injected hydrocarbon gases in general tend to have better recovery efficiency, due to their superior competitive adsorption capability.

The conclusion drawn from this work can be applied to the field development optimization of shale and tight reservoirs, and can be extended to the assessment of carbon storage in depleted unconventional reservoirs.

Admittedly, this work has several limitations. Firstly, we didn't simulate hydrocarbon components that are heavier than decane. As such, the 'sieving' effect [5] induced by the long-chain hydrocarbon structure is not obvious. Secondly, our analysis of the phase behavior is still based on conventional equation of state. Thirdly, we restrict our

analysis to slit-like nano channels. Spherical shape nano channel should have higher impacts on the differential release/retention of hydrocarbons. Fourthly, limited by the computational capability, our MD simulation is based on a single nano pore. Looking forward, we propose to further probe the transport of heavier components, such as asphaltene, using the nano scale phase equilibrium calculation [18] approach in a more complex porous system.

## **Declaration of Competing Interest**

The authors declare that they have no known competing financial interests or personal relationships that could have appeared to influence the work reported in this paper.

#### Data availability

Data will be made available on request.

## Acknowledgement

RQ acknowledges the partial support from NSF under grant number CBET-2246274.

#### Appendix A. Equation of state

In this appendix, we present the formulations of the PR-EOS we used for the calculation of the compositional profile shown in Fig. 9. In our work, we also adopt a confined equation of state [32].

In PR-EOS, the pressure *P* of the phase is calculated as below

$$P = \frac{RT}{V_m - b} - \frac{\alpha a}{V_m^2 + 2bV_m - b^2} \tag{A1}$$

In the above equation, R and T is the gas constant and temperature, respectively.  $V_m$  is the molar volume. The parameter a and b are calculated by the following mixing rules.

$$a = \sum \sum x_i x_j a_{ij} \tag{A2}$$

$$b = \sum x_i b_i \tag{A3}$$

Where  $x_i$  and  $x_i$  is the mole fraction of the ith and jth hydrocarbon component, respectively.

 $a_{ij}$  is defined as

$$a_{ij} = \left(1 - k_{ij}\right)\sqrt{a_i a_j} \tag{A4}$$

where

$$a_i = 0.45724 \left( RT_{C,i} \right)^2 / P_{c,i} \cdot \left( 1 + \kappa_i \left( 1 - \sqrt{T/T_{c,i}} \right) \right)^2$$
 (A5)

$$\kappa_i = -0.26992w_i^2 + 1.54226w_i + 0.37464 \tag{A6}$$

Meanwhile,  $b_i$  is defined as

$$b_i = 0.0778RT_{Ci}/P_{ci} (A7)$$

In the above equations,  $T_{C,i}$ ,  $P_{c,i}$  and  $w_i$  is the critical temperature, critical pressure and acentric factor of component i, respectively.

 $k_{ij}$  in Eq. (A4) is the binary interaction factor between component i and component j. We have the relationship  $k_{ij} = k_{ji}$ .

In this work, the critical temperature, critical pressure and acentric factor for methane are set to be 190.56 K, 4599 kPa, and 0.0115 respectively, while the same properties for decane are set as 617.7 K, 2110 kPa, and 0.4923 respectively. The binary interaction coefficient between the two components is 0.05. The above parameters are from [41]. We use Rachford-Rice equation approach [42] with Gibbs energy-based stability tests [43] to obtain the phase envelop in Fig. 9.

It should be noted that in our work we also use an equation of state which considers the confinement effect to estimate the initial status of the MD system. This confinement equation of state is developed by Luo et al. [32] by augmenting the PR-EOS with a pore-size dependent term to represent the wall impact. The confinement EOS requires a global energy minimization approach in the phase equilibrium calculation. Due to the complexity of the formulations, we omit the descriptions of the equations in this paper. Interested readers can refer to [32]. Since the confinement EOS assumes the nano pore is in instant equilibrium with the bath pore, it cannot be used to calculate the phase behavior during the recovery (with flow dynamic) process, but can only be used when the system is in equilibrium. This is why we use it for the estimation of the initial status of the MD system.

## References

- M.E. Best, T.J. Katsube, Shale permeability and its significance in hydrocarbon exploration, Lead. Edge 14 (1995) 165–170, https://doi.org/10.1190/1.1437104.
- [2] B. Grieser, J. Bray, Identification of production potential in unconventional reservoirs, OnePetro (2007), https://doi.org/10.2118/106623-MS.
- [3] D. Alfarge, M. Wei, B. Bai, IOR methods in unconventional reservoirs of North America: comprehensive review, OnePetro (2017), https://doi.org/10.2118/ 195600 MS
- [4] J. Shi, L. Gong, S. Sun, Z. Huang, B. Ding, J. Yao, Competitive adsorption phenomenon in shale gas displacement processes, RSC Adv. 9 (2019) 25326–25335, https://doi.org/10.1039/C9RA04963K.
- [5] Z. Zhu, C. Fang, R. Qiao, X. Yin, E. Ozkan, Experimental and molecular insights on mitigation of hydrocarbon sieving in Niobrara Shale by CO2 Huff 'n' Puff, SPE J. 25 (2020) 1803–1811, https://doi.org/10.2118/196136-PA.
- [6] S. Wang, Y. Zhang, H. Wu, S.H. Lee, R. Qiao, X.-H. Wen, A kinetic model for multicomponent gas transport in shale gas reservoirs and its applications, Phys. Fluids 34 (2022), 082002, https://doi.org/10.1063/5.0101272.
- [7] D.Y. Moh, H. Zhang, S. Wang, X. Yin, R. Qiao, Soaking in CO2 huff-n-puff: A single-nanopore scale study, Fuel 308 (2022), 122026, https://doi.org/10.1016/j.fuel.2021.122026.
- [8] S. Wang, X. Yao, Q. Feng, F. Javadpour, Y. Yang, Q. Xue, et al., Molecular insights into carbon dioxide enhanced multi-component shale gas recovery and its

- sequestration in realistic kerogen, Chem. Eng. J. 425 (2021), 130292, https://doi.org/10.1016/j.cej.2021.130292.
- [9] J. Liu, Y. Yang, S. Sun, J. Yao, J. Kou, Flow behaviors of shale oil in kerogen slit by molecular dynamics simulation, Chem. Eng. J. 434 (2022), 134682, https://doi. org/10.1016/j.cej.2022.134682.
- [10] M. Zhang, S. Zhan, Z. Jin, Recovery mechanisms of hydrocarbon mixtures in organic and inorganic nanopores during pressure drawdown and CO2 injection from molecular perspectives, Chem. Eng. J. 382 (2020), 122808, https://doi.org/ 10.1016/j.cej.2019.122808.
- [11] Y. Zhao, W. Li, S. Zhan, Z. Jin, Breakthrough pressure of oil displacement by water through the ultra-narrow kerogen pore throat from the Young-Laplace equation and molecular dynamic simulations, PCCP 24 (2022) 17195–17209, https://doi. org/10.1039/D2CP01643F
- [12] S. Luo, J.L. Lutkenhaus, H. Nasrabadi, Effect of nanoscale pore-size distribution on fluid phase behavior of gas-improved oil recovery in shale reservoirs, SPE J. 25 (2020) 1406–1415, https://doi.org/10.2118/190246-PA.
- [13] Y. Yang, J. Zhang, L. Xu, P. Li, Y. Liu, W. Dang, Pore Structure and Fractal Characteristics of Deep Shale: A Case Study from Permian Shanxi Formation Shale, from the Ordos Basin, ACS Omega 7 (2022) 9229–9243, https://doi.org/10.1021/ acsomega.1c05779.
- [14] J. Berthonneau, A. Obliger, P.-L. Valdenaire, O. Grauby, D. Ferry, D. Chaudanson, et al., Mesoscale structure, mechanics, and transport properties of source rocks' organic pore networks, Proc. Natl. Acad. Sci. 115 (2018) 12365–12370, https://doi.org/10.1073/pnas.1808402115.

- [15] D.D. Cramer, Stimulating unconventional reservoirs: lessons learned, successful practices, areas for improvement, OnePetro (2008), https://doi.org/10.2118/ 114172\_MS
- [16] Y. Song, Z. Li, Z. Jiang, Q. Luo, D. Liu, Z. Gao, Progress and development trend of unconventional oil and gas geological research, Pet. Explor. Dev. 44 (2017) 675–685, https://doi.org/10.1016/S1876-3804(17)30077-0.
- [17] X. Hong, H. Xu, H. Yu, X. Jin, H. Liu, F. Wang, et al., Molecular understanding on migration and recovery of shale gas/oil mixture through a pore throat, Energy Fuels (2022), https://doi.org/10.1021/acs.energyfuels.2c03315.
- [18] R.G. Loucks, R.M. Reed, S.C. Ruppel, U. Hammes, Spectrum of pore types and networks in mudrocks and a descriptive classification for matrix-related mudrock pores, AAPG Bull. 96 (2012) 1071–1098, https://doi.org/10.1306/08171111061.
- [19] S. Thomas, Enhanced Oil Recovery An Overview, Oil Gas Sci. Technol. Rev. IFP 63 (2008) 9–19, https://doi.org/10.2516/ogst:2007060.
- [20] D.W. Green, G.P. Willhite, Enhanced Oil Recovery (2018), https://doi.org/ 10.2118/9781613994948.
- [21] S. Luo, J.L. Lutkenhaus, H. Nasrabadi, Confinement-Induced Supercriticality and Phase Equilibria of Hydrocarbons in Nanopores, Langmuir 32 (2016) 11506–11513, https://doi.org/10.1021/acs.langmuir.6b03177.
- [22] S. Riewchotisakul, I.Y. Akkutlu, Adsorption-Enhanced Transport of Hydrocarbons in Organic Nanopores, SPE J. 21 (2016) 1960–1969, https://doi.org/10.2118/ 175107-PA.
- [23] H. Ghasemzadeh, S. Babaei, S. Tesson, J. Azamat, M. Ostadhassan, From excess to absolute adsorption isotherm: The effect of the adsorbed density, Chem. Eng. J. 425 (2021), 131495, https://doi.org/10.1016/j.cej.2021.131495.
- [24] B. Liu, S. Babaei, L. Bai, S. Tian, H. Ghasemzadeh, M. Rashidi, et al., A dilemma in calculating ethane absolute adsorption in shale gas reservoirs: A theoretical approach, Chem. Eng. J. 450 (2022), 138242, https://doi.org/10.1016/j. cei.2022.138242.
- [25] H. Wu, Y. He, R. Qiao, Recovery of Multicomponent Shale Gas from Single Nanopores, Energy Fuels 31 (2017) 7932–7940, https://doi.org/10.1021/acs. energyfuels 7301013
- [26] H. Wu, Y. He, R. Qiao, Superdiffusive gas recovery from nanopores, Phys. Rev. Fluids 1 (2016), 074101, https://doi.org/10.1103/PhysRevFluids.1.074101.
- [27] M. Barisik, A. Beskok, Scale effects in gas nano flows, Phys. Fluids 26 (2014), 052003, https://doi.org/10.1063/1.4874678.
- [28] M.G. Martin, J.I. Siepmann, Transferable Potentials for Phase Equilibria. 1. United-Atom Description of n-Alkanes, J. Phys. Chem. B 102 (1998) 2569–2577, https://doi.org/10.1021/jp972543+.

- [29] V.V. Pisarev, S.A. Zakharov, Comparison of forcefields for molecular dynamics simulations of hydrocarbon phase diagrams, J. Phys. Conf. Ser. 946 (2018), 012100, https://doi.org/10.1088/1742-6596/946/1/012100.
- [30] F.N. Mendoza, R. López-Rendón, J. López-Lemus, J. Cruz, J. Alejandre, Surface tension of hydrocarbon chains at the liquid-vapour interface, Mol. Phys. 106 (2008) 1055–1059, https://doi.org/10.1080/00268970802119694.
- [31] M. Alfi, H. Nasrabadi, D. Banerjee, Effect of Confinement on Bubble Point Temperature Shift of Hydrocarbon Mixtures: Experimental Investigation Using Nanofluidic Devices, OnePetro (2017), https://doi.org/10.2118/187057-MS.
- [32] S. Luo, B. Jin, J.L. Lutkenhaus, H. Nasrabadi, A novel pore-size-dependent equation of state for modeling fluid phase behavior in nanopores, Fluid Phase Equilib. 498 (2019) 72–85, https://doi.org/10.1016/j.fluid.2019.06.009.
- [33] A.P. Thompson, H.M. Aktulga, R. Berger, D.S. Bolintineanu, W.M. Brown, P. S. Crozier, et al., LAMMPS a flexible simulation tool for particle-based materials modeling at the atomic, meso, and continuum scales, Comput. Phys. Commun. 271 (2022), 108171, https://doi.org/10.1016/j.cpc.2021.108171.
- [34] D.J. Evans, B.L. Holian, The Nose-Hoover thermostat, J. Chem. Phys. 83 (1985) 4069–4074, https://doi.org/10.1063/1.449071.
- [35] L. Martínez, R. Andrade, E.G. Birgin, J.M. Martínez, PACKMOL: A package for building initial configurations for molecular dynamics simulations - Martínez -2009, J. Comput. Chem. - Wiley Online Library J. Comput. Chem. 30 (2009) 2157–2164, https://doi.org/10.1002/jcc.21224.
- [36] D.-Y. Peng, D.B. Robinson, A New Two-Constant Equation of State, Ind. Eng. Chem. Fundam. 15 (1976) 59–64, https://doi.org/10.1021/i160057a011.
- [39] J. Wang, T. Hou, Application of molecular dynamics simulations in molecular property prediction II: Diffusion coefficient, J. Comput. Chem. 32 (2011) 3505–3519, https://doi.org/10.1002/jcc.21939.
- [40] D.Y. Moh, H. Zhang, S. Sun, R. Qiao, Molecular anatomy and macroscopic behavior of oil extraction from nanopores by CO2 and CH4, Fuel 324 (2022), 124662, https://doi.org/10.1016/j.fuel.2022.124662.
- [41] Properties of Gases and Liquids. 5th Edition. McGraw-Hill Education; 2001.
- [42] C.F. Leibovici, J. Neoschil, A solution of Rachford-Rice equations for multiphase systems, Fluid Phase Equilib. 112 (1995) 217–221, https://doi.org/10.1016/0378-3812(95)02797-I.
- [43] M.L. Michelsen, The isothermal flash problem. Part i. Stability, Fluid Phase Equilibria 9 (1982) 1–19. https://doi.org/10.1016/0378-3812(82)85001-2.